Synthetic fluid inclusions XX. Critical PTx properties of H2O–FeCl2 fluids

ARTICLE *in* GEOCHIMICA ET COSMOCHIMICA ACTA · JANUARY 2014

Impact Factor: 4.33 · DOI: 10.1016/j.gca.2014.09.026

3 AUTHORS, INCLUDING:

Pilar Lecumberri-Sanchez

ETH Zurich

8 PUBLICATIONS **66** CITATIONS

SEE PROFILE

Robert Bodnar

Virginia Polytechnic Institute and State Uni…

352 PUBLICATIONS **7,730** CITATIONS

SEE PROFILE

Available online at www.sciencedirect.com

ScienceDirect

Geochimica et Cosmochimica Acta 148 (2015) 50–61

Geochimica et Cosmochimica Acta

www.elsevier.com/locate/gca

Synthetic fluid inclusions XX. Critical *PTx* properties of H_2O–$FeCl_2$ fluids

Matthew Steele-MacInnis [*,1], Pilar Lecumberri-Sanchez [1], Robert J. Bodnar

Department of Geosciences, Virginia Tech, Blacksburg, VA 24061, USA

Received 26 May 2014; accepted in revised form 16 September 2014; available online 2 October 2014

Abstract

Iron chloride is a common and abundant component in hydrothermal fluids in many geologic environments, yet the thermodynamic and *PTx* properties of $FeCl_2$-bearing aqueous fluids are poorly known. In this study we have used the synthetic fluid inclusion technique to characterize the *PTx* conditions along the critical curve of the system H_2O–$FeCl_2$. For a given temperature or salinity, the critical pressure in the H_2O–$FeCl_2$ system is lower than that in the H_2O–NaCl system. In contrast, the critical curves of aqueous solutions of other divalent-cation chlorides, such as $MgCl_2$ and $CaCl_2$, are at higher pressure than that of NaCl solutions of equivalent temperature or salinity. The results of this study provide the first quantitative constraints on the *PTx* extent of liquid–vapor immiscibility for $FeCl_2$-rich fluids. Owing to the low pressure along the critical curve compared to other common aqueous chloride systems, immiscibility of $FeCl_2$-rich fluids appears to be limited to relatively low pressures, or relatively shallow levels in the crust, compared to other saline hydrothermal fluids.

1. INTRODUCTION

Iron chloride is among the most abundant components in magmatic-hydrothermal fluids in a variety of geologic environments (Yardley, 2005; Bodnar et al., 2014; Yardley and Bodnar, 2014). Early qualitative reports of iron chloride-rich fluids include the fluid inclusion (FI) studies of Bolivian porphyry Sn deposits by Grant et al. (1977). Grant et al. (1977) observed hydrous iron chloride daughter minerals in fluid inclusions from these deposits, and the volumetric phase ratios of the FI suggested that the hydrothermal fluids contained higher concentrations of $FeCl_2$ than NaCl (Roedder, 1984). Roedder (1984) also noted that iron is commonly the most abundant metal in FI from porphyry copper deposits. In recent years, advances in microanalytical techniques applied to fluid inclusions (such as laser ablation ICPMS; Günther et al., 1998) have permitted direct quantification of the compositions of hydrothermal fluids. Such analyses have shown that iron concentrations in natural fluids generally increase with increasing temperature, reaching several weight percent (wt%) iron in fluids above 400 °C (Yardley, 2005). Iron chloride concentrations of up to several tens of wt% have been reported in granite-related Sn–W deposits (e.g., Audétat et al., 2000; Kamenetsky et al., 2002). Iron concentrations of several wt% have also been observed in FI in hydrothermal veins within the Sudbury complex, where solid $FeCl_2$ (lawrencite) occurs as an accessory phase included in sulfides associated with these veins (Hanley et al., 2005). Iron concentrations in fluids from submarine ("black-smoker") hydrothermal systems are generally on the order of a few tenths of a wt%, and measured Fe concentrations (when coupled with Mn contents) provide a

* Corresponding author. Tel.: +41 44 632 39 09; fax: +41 44 632 18 27.

E-mail addresses: steele-macinnis@erdw.ethz.ch (M. Steele-MacInnis), pilar@erdw.ethz.ch (P. Lecumberri-Sanchez), rjb@vt.edu (R.J. Bodnar).

[1] Present address: Institute for Geochemistry and Petrology, Clausiusstrasse 25, CH-8092 Zürich, Switzerland.

http://dx.doi.org/10.1016/j.gca.2014.09.026
0016-7037/

useful thermometer for assessing sub-seafloor conditions in these systems (Pester et al., 2011).

Liquid–vapor immiscibility (sometimes referred to as "boiling" in the literature) commonly plays a significant role in magmatic-hydrothermal processes, for example controlling the transport and partitioning of metals, as well as influencing pH and oxygen fugacity (Drummond and Ohmoto, 1980). Thus, precipitation of ore minerals is commonly related to the occurrence of immiscibility in magmatic-hydrothermal systems (e.g., Drummond and Ohmoto, 1980; Hedenquist and Lowenstern 1994; Hedenquist et al., 1998; Moncada et al., 2012). In addition, some alteration mineral assemblages, such as advanced-argillic alteration, are considered to represent alteration of original rock minerals by acidic fluids produced by liquid–vapor immiscibility (Hedenquist and Lowenstern, 1994).

Fluid inclusions commonly provide the best evidence of immiscibility in magmatic-hydrothermal systems. Assemblages of coexisting vapor-rich and liquid-rich or halite-bearing (brine) inclusions represent trapping of coexisting immiscible fluids, and the homogenization temperatures of such FI represent the formation temperature (Roedder, 1984). The formation pressure can then be deduced from the formation temperature, based on experimentally determined *PTx* liquid–vapor equilibria for model fluid systems.

The significance of iron chloride as a major component in magmatic-hydrothermal systems for the physical and chemical properties of ore-forming fluids cannot currently be evaluated, owing to the limited experimental data that are available for iron-bearing fluids (Liebscher, 2007). Addition of chloride salts to aqueous solution dramatically expands the pressure–temperature (*PT*) region of liquid–vapor immiscibility. The best-studied binary system in this regard is H_2O–NaCl (e.g., Souririjan and Kennedy, 1962; Bischoff and Pitzer, 1989; Bodnar et al., 1985; Shmulovich et al., 1995), for which the extent of liquid–vapor immiscibility has been extensively characterized up to ~1000 °C (see Driesner and Heinrich, 2007, and references therein). Other geologically relevant H_2O–salt systems for which the L–V equilibria have been at least partially characterized include H_2O–KCl, H_2O–$CaCl_2$ and H_2O–$MgCl_2$ (e.g., Oakes et al., 1994; Dubois et al., 1994; Shmulovich et al., 1995; see Liebscher, 2007, for a review and comparison of L–V equilibria in these and other binary systems, and Valyashko, 2014, for a comprehensive summary of available experimental *PVTx* data for all aqueous systems). In comparison with these systems, the *PTx* conditions of L–V equilibrium in the system H_2O–$FeCl_2$ are virtually unknown.

One of the key topological features of binary phase equilibria is the pressure-temperature-composition (*PTx*) trajectory of the locus of critical points, which is usually referred to as the critical curve. For any given temperature, the critical curve represents the highest possible pressure at which L–V immiscibility can occur (Fig. 1a). Stated differently, at pressures above the critical curve (at a given temperature), the fluid is always in the single-phase state, whereas immiscibility may occur at lower pressures (depending also on the bulk composition). As such, knowledge of the *PTx* trajectory of the critical curve provides quantitative constraints on the *PTx* conditions at which liquid–vapor immiscibility may occur which, in turn, may used to predict in which geologic settings we might expect immiscible fluids if the bulk fluid composition is Fe-rich.

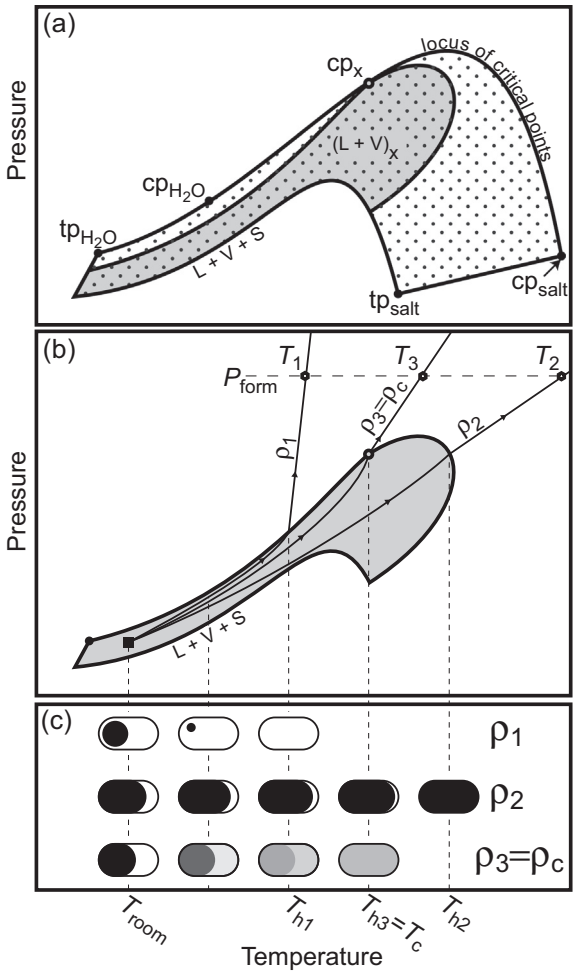

Fig. 1. Schematic representation of the procedure used to locate *PTx* points along the critical curve. (a) Topology of a binary H_2O-"salt" system with a continuous critical curve. The stippled region represents the *PT* projection of the entire region over which L–V immiscibility is possible, bounded by the liquid–vapor curves of the two end-members (from the two triple points, tp_{H2O} and tp_{salt}, to the two critical points, cp_{H2O} and cp_{salt}), the three-phase liquid + vapor + solid curve (from tp_{H2O} to tp_{salt}), and the critical curve (from cp_{H2O} to cp_{salt}). The shaded region represents the conditions of L-V immiscibility for a specific bulk composition. The point labelled cp_x represents the critical point for this bulk composition. (b) Heating paths followed by FI synthesized at pressure = P_{form} and temperatures = T_1, T_2 and T_3. c) Phase changes observed during heating in the FI synthesized at the three conditions shown in (b). The inclusion formed at T_1 homogenizes to the liquid at T_{h1}; the inclusion formed at T_2 homogenizes to the vapor at T_{h2}; the inclusion formed at T_3 has the critical density and homogenizes by critical phenomena at $T_{h3} = T_c$ (the critical temperature, for this composition).

Previously, Knight and Bodnar (1989) used the synthetic fluid inclusion technique (Sterner and Bodnar, 1984) to determine conditions along the critical curve of the system

H_2O–NaCl. Later, Oakes et al. (1994) used a similar approach to characterize part of the critical curve of the system H_2O–$CaCl_2$. In the present study, we use this approach to investigate the locus of critical points, hereafter referred to as the critical curve, of the system H_2O–$FeCl_2$.

2. METHODS

2.1. Fluid Inclusion synthesis

Fluid inclusions were synthesized according to procedures described by Sterner and Bodnar (1984) and Bodnar and Sterner (1987). Additional considerations related to synthesis of $FeCl_2$-bearing FI, especially the role of redox state and alloying with the capsule material, have been described by Lecumberri-Sanchez et al. (2015). Here, we briefly describe the experimental method, focusing on those aspects that are specific to experiments involving iron-bearing fluids.

Experiments were conducted using either Au or Pt capsules (for reasons described in Section 3, below). The capsules were loaded with a pre-fractured quartz core, plus approximately 60 μL of aqueous $FeCl_2$ solution (10, 15, 20, 25, 30 or 35 wt% $FeCl_2$) prepared from de-oxygenated, doubly distilled water plus analytical grade $FeCl_2{\cdot}4H_2O$ granules (Alpha Aesar). The solutions loaded into the capsules characteristically had a green color, indicating that the solution contained ferrous (Fe^{2+}) (rather than ferric) iron. The solutions were prepared immediately prior to loading the capsules, because we found that after the solutions were exposed to air for ~6–7 h the iron would begin to oxidize to ferric iron (Fe^{3+}), as indicated by the formation of a reddish-orange particulate (either suspended in the liquid, or settled on the bottom of the glass vial). Such partially oxidized solutions were not used for the experiments and were discarded.

After loading, the capsules were sealed with an arc welder and the sealed capsules were placed into cold-seal pressure vessels. Experiments were run at 500–3000 bar and 400–700 °C for 7–14 days. Temperature was monitored using a chromel-alumel type thermocouple that was inserted into a small hole drilled into the end of each pressure vessel such that the tip of the thermocouple was within ~1 cm of the capsule, and pressure was monitored using a Bourdon-type Heise gauge. The cold-seal vessels were constructed of René 41 (Ni–Cr–Mo–Co–Al–Ti alloy) and the pressure medium was water containing a small amount of water-soluble oil to minimize corrosion; thus the experiments were buffered at an oxygen fugacity of Ni–NiO (NNO) (Eugster and Skippen, 1967; Popp et al., 1984; Frank et al., 2001).

Healed quartz cores containing synthetic FI from the experiments were prepared using the procedures described by Sterner and Bodnar (1984). Microthermometric measurements were conducted using a USGS-type gas-flow stage (Werre et al., 1979) for temperatures below 500 °C, or a Linkam TS1400XY stage (Esposito et al., 2012) for temperatures above 500 °C. Temperature in the gas-flow stage was calibrated using synthetic fluid inclusions according to the triple points of CO_2 (−56.6 °C) and H_2O (0.0 °C) and the critical point of H_2O (374.1 °C); temperature in the Linkam stage was calibrated according to the H_2O critical point, the 1-atm α–β transition of quartz (574 °C) and the triple point of NaCl (801 °C).

2.2. Strategy for determining critical *PTx* conditions

The procedure for determining conditions along the critical curve using synthetic fluid inclusions, first described by Knight and Bodnar (1989) and later by Oakes et al. (1994), is shown schematically in Fig. 1. In this procedure, the first step is to define two or more *PT* points along the critical isochore for each given bulk composition. The critical isochore is defined by the locus of two or more *PT* points at which a fluid of a given composition has the critical density. Over short intervals of *P* and *T* the critical isochore is assumed to be a straight line, and the line defined by the two (or more) points is then extrapolated to the measured critical homogenization temperature (which should be identical for the two (or more) samples in which inclusions were trapped at different *PT* points along the critical isochore) to obtain the critical pressure. The locus of critical points thus represented by fluids with different salinities or concentrations defines the critical curve in the binary system.

Each *PT* point along the critical isochore for a given composition is obtained by synthesizing fluid inclusions at various temperatures along an isobar (P_{form} in Fig. 1b). Inclusions formed at temperatures lower than the temperature on the critical isochore will trap a fluid of liquid-like density (i.e., density > critical density), and such FI will have a relatively small vapor bubble at room temperature and will homogenize to the liquid phase during heating by shrinking and disappearance of the vapor bubble at T_h (FI with density ρ_1 in Fig. 1c). Inclusions formed at temperatures higher than the temperature on the critical isochore at the pressure of the isobar, and at pressures above the liquid + vapor field at that temperature, will have a vapor-like density (i.e., density < critical density) and homogenize to the vapor phase by expansion of the vapor bubble to fill the inclusion at T_h (FI with density ρ_2 in Fig. 1c).

For each given composition, there is only one temperature along the isobar at which trapped fluid inclusions will have the critical density. These inclusions will neither homogenize by shrinkage and disappearance of the vapor bubble, nor by expansion of the vapor bubble to fill the inclusion at T_h, but rather will homogenize by fading of the meniscus between liquid and vapor (Fig. 2). Therefore, initial "reconnaissance" experiments are conducted using a fairly coarse temperature grid along each isobar to bracket the temperature along the critical isochore for a given pressure and composition. Synthetic fluid inclusions from the reconnaissance experiments are examined petrographically and by microthermometry, with the highest formation temperature at which inclusions homogenize to the liquid phase, and the lowest formation temperature at which inclusions homogenize to the vapor phase bracketing the critical isochore. In subsequent experiments, inclusions are synthesized at temperatures between these two bounding temperatures, using decreasing temperature steps for each iteration. Usually only 2 or 3 iterations were necessary to produce inclusions along a given isobar that

homogenized by critical behavior. It is thus possible to synthesize FI at the precise temperature (along an isobar) where fluids have the critical density (for the given composition) and the trapped inclusions therefore homogenize by critical phenomena (FI with density $\rho_3 = \rho_c$ in Fig. 1c). The homogenization temperature of such FI represents the critical temperature for this composition. By repeating this procedure along a second (or more) isobar, one can identify two points along the critical isochore, and linear extrapolation of the trend in these data to the measured critical temperature constrains the critical pressure. This process is repeated for other bulk compositions (salinities) to provide a series of *PTx* points along the critical curve.

As described by Oakes et al. (1994), several factors affect the precision of the technique described above. Firstly, critical homogenization (fading of the meniscus between liquid and vapor) only occurs for FI with exactly the critical density. However, in practice this style of homogenization may appear to occur for FI that have densities that are "close" to the critical density. Inclusions with density close (but not equal) to the critical density may appear to homogenize by critical phenomena because the L–V solvus becomes "flat" in temperature (T)–density (ρ) space such that $dT/d\rho$ approaches zero near the critical point (see Roedder, 1984). Furthermore, the precision with which the critical isochore can be located depends on the difference between the formation pressure and the critical pressure. For example, if the formation $P \gg P_c$ (i.e., formation pressure significantly greater than the critical pressure), then there will be a range of formation temperatures of several 10's of °C, within which the density is "near" critical and homogenization appears to occur by fading of the meniscus (because the isochores diverge with increasing pressure). Such a wide range of formation temperatures that produce fluid inclusions with near-critical density at $P \gg P_c$ is advantageous in the early "reconnaissance" stage, because it increases the likelihood of synthesizing fluid inclusions of near-critical density. However, such ranges of formation temperatures with near-critical densities are disadvantageous for precisely constraining the *PT* trajectory of the critical isochore because of the increased uncertainty in the temperature on the critical isochore at the pressure corresponding to the isobar. Thus, the critical isochore is more precisely constrained by experiments in which fluid inclusions are trapped at P only slightly greater than P_c (i.e., where density variation with T is greatest). Therefore, in the present study, we obtained at least three points along some of the critical isochores (to improve the statistics of the linear approximation), and we attempted to locate points on the critical isochores at P close to P_c. Despite these protocols, each measurement includes a finite uncertainty, which we have propagated to estimate the uncertainty in the *PTx* conditions along the H_2O–$FeCl_2$ critical curve.

3. RESULTS

3.1. Low-temperature microthermometric measurements

Compositional modification in iron-bearing hydrothermal experiments is commonly reported in the literature (e.g., Fe alloying with the capsule material: Bowen and Schairer, 1932; Zajacz et al., 2011; redox reactions and/or magnetite precipitation: Chou and Eugster, 1977), and described in more detail by Lecumberri-Sanchez et al. (2015). Thus, modification of the bulk composition by one or more of these processes could not be ruled out *a priori*, and was assessed after each experiment. Therefore, before conducting high-temperature microthermometric measurements, FI were analyzed by low-temperature microthermometry. We compared the last ice dissolution temperatures ($T_{m,ice}$) with the known vapor-saturated liquidus phase relations (as summarized by Linke, 1958), to check for any signs of compositional modification of the fluid during the inclusion synthesis experiments.

Low-temperature microthermometric properties of the FI analyzed in this study have been previously summarized by Lecumberri-Sanchez et al. (2015), and are shown in Fig. 3. FI synthesized using the same starting composition, but formed at different temperatures and pressures (~400–700 °C and 500–3000 bar) show variation of $T_{m,ice}$ between samples of about ±1 to ±3 °C (Table 1). The measured ice dissolution temperatures were consistent with previously published data along the vapor-saturated ice liquidus of the system H_2O–$FeCl_2$ (Linke, 1958). FI of 30 wt% $FeCl_2$ (the approximate eutectic liquid composition) exhibited an average last ice dissolution of −37.2 °C, in agreement with the published eutectic temperature of −37 °C (Schimmel, 1928). FI containing 35 wt% $FeCl_2$ (in which the last solid phase to dissolve should be $FeCl_2 \cdot 6H_2O$, at equilibrium; Linke, 1958) could not be solidified, and remained in the super-cooled liquid state even when cooled to −196 °C. We did not observe any systematic variation of $T_{m,ice}$ with formation temperature or pressure. In addition there was no systematic difference between FI synthesized in Au versus Pt capsules (Table 1). These results suggest that $FeCl_2$ concentrations remained essentially constant throughout our experiments (Lecumberri-Sanchez et al., 2015), contrary to what we would expect if some Fe were lost from the fluid by alloying with the Pt capsule material. This, in turn, suggests that Fe–Pt alloying did not occur. Alternatively, it is possible that Fe–Pt alloying occurred to some extent, but on timescales longer than required for fracture healing and fluid inclusion entrapment at the conditions of our experiments (such that the compositions of the FI represent the fluid compositions at the start of each experiment). For additional discussion of these issues, the reader is referred to Lecumberri-Sanchez et al. (2015).

3.2. Critical isochores and critical curve of H_2O–$FeCl_2$ fluids

The bracketing approach described in Section 2.2 commonly requires several experiments to locate conditions along the critical isochores. In the following, we exclude the early "reconnaissance" experiments that initially helped us to bracket the required formation temperature for the critical isochore, and focus on those results that provide constraints on the critical isochores (i.e., FI exhibiting critical or near-critical homogenization, as well as closely-spaced experiments bracketing the critical isochores).

Table 1
PTX and microthermometric data used to construct isochores of the critical density for H_2O–$FeCl_2$ fluids.

Exp. ID	Salinity (wt% $FeCl_2$)	P_{form} (bar)	T_{form} (°C)	$T_{m,ice}$ (°C)	± (°C)	*n*	$T_{h,LV}$ (°C)	± (°C)	homog. to[a]	*n*
	0			0.0			374.1[b]		Cr	
032112-viii	10	500	450	−6.0	0.1	7	405.0	2.0	L	7
071413-xli	10	500	461				416	2.0	Cr	5
032112-vi	10	500	500	−6.0	0.4	4	497.0	1.5	V	4
032112-xiii	10	750	500	−5.9	0	5	399.6	0.7	L	5
071413-xliii	10	750	515				398	4	L < Cr	5
032112-xiv	10	750	549	−6.3	0	4	436	1	V	4
120811-xii	10	1100	450	−5.4	0.1	3	349.8	0.1	L	3
120811-xiv	10	1500	600	−5.9	0.1	3	384.4	0.3	L	3
051712-xx	15	500	450				406.5	0.1	L	3
071413-xliv	15	500	461				418.8	1.2	L < Cr	8
071313-xxx	15	500	475				460	5	V	6
051712-xix	15	500	500				504	5	V	5
071313-xxvii	15	750	527				428	3	Cr < V	6
051712-vix	15	750	550				467	0	V	4
051712-x	15	750	600						2Φ	
051712-xvii	15	1000	550				410	0.5	L < Cr	6
051712-xi	15	1000	575				418	0	L < Cr	4
071313-xxxiv	15	1000	585				483	8	V	9
051712-xvi	15	1000	600				438	0	V	4
051712-xiv	15	2000	700				394	0	L	7
012812-vii	15	2000	400	−8.4	0	4	272.2	0	L	4
012812-iv	15	2000	600	−9.0	0	4	372	0.2	L	4
012812-ix	15	3000	500	−8.4	0	2	291.4	0	L	2
012812-v	15	3000	600	−9.8	0	3	340.2	0	L	3
032112-xxi	20	500	450	−16.7	0.1	3	428	0.2	L	3
080112-vi	20	500	473				456	4	Cr < V	7
032112-xxii	20	500	500	−18.3	0.1	5	492	2	V	3
032112-xxiii	20	750	500	−17.1	0.2	4	434	0.3	L	4
071413-xl	20	750	515				434	1.1	Cr	4
080112-vii	20	750	525				459	0	Cr < V	6
032512-xxxv	20	750	550	−18.3	0.3	5	503	10	V	5
032112-xix	20	750	600	174[d]	4	3	602	2	2Φ	7
032112-xv	20	1000	500	−16	0.2	3	400.0	0.1	L	3
032512-xxxiv	20	1000	550	−18.3	0.1	4	411.8	0.1	L	4
080112-iv	20	1000	575				435	0.9	Cr	4
032512-vix	20	1000	600	−17.7	0	2	470	5	V	2
120911-xxx	20	1500	500	−17.4	0	2	362.5	0.5	L	6
120911-xxxv	20	1500	535	−17.2	0	5	384.5	1	L	5
120911-xxiii	20	1500	600	−18.7	0.1	4	396.9	1.5	L	4
120212-xxxi	20[c]	1500	600				405.2	0.1	L	3
080112-iii	20	1500	689				438	2	L < Cr	4
051712-xxix	25	500	500				498	1.0	2Φ	5
071313-xxxii	25	515	510				515	15	2Φ	7
071313-xxxiii	25	1250	630				458	3	Cr < V	3
012912-xviii	25	2000	400	−24.0	0.2	2	292	0	L	2
080212-xvi	30	500	473				463	1.1	L	4
080212-xv	30	500	508						2Φ	
032212-xxiv	30	500	550						2Φ	
032212-xxxi	30	750	550	−37.4	0	5	503		L < Cr	
080212-xvii	30	750	553				555	1.5	2Φ	6
120112-iii	30[c]	750	553				567	5	2Φ	6
032212-xxx	30	750	600	187[d]	0.5	3	603	1	2Φ	3
032212-xxxvii	30	1000	550	−39.6	0.2	2	425.6	0.1	L	2
032212-xxxix	30	1000	600	−38.5	0.5	5	508	0	Cr	5
120112-i	30[c]	1000	600				519	5	Cr < V	5
080212-xiv	30	1240	650				506.1	0.3	Cr < V	4
120811-iv	30	1500	650				479.1	5	L < Cr	3
080212-xviii	30[c]	1500	689				484	1.5	L < Cr	5

Table 1 (*continued*)

Exp. ID	Salinity (wt% $FeCl_2$)	P_{form} (bar)	T_{form} (°C)	$T_{m,ice}$ (°C)	± (°C)	*n*	$T_{h,LV}$ (°C)	± (°C)	homog. to[a]	*n*
032212-xxv	30	1993	600	−37.0	0	2	400.7	0.3	L	2
012912-xiv	35	2000	600	dnf			411.5	0.3	L	2
012912-xiii	35	2000	700	dnf			451.3	0.1	L	2
060312-lii	63.6	500	508	219[d]	0.3	6	505.4	2	L	6
060312-li	63.6	750	535	220[d]	0.2	6	529.6	0	L	6

[a] Mode of homogenization of the FI; to the liquid (L) or vapor (V) phase, or by critical phenomena (Cr). L < Cr denotes near-critical homogenization to the liquid phase, and Cr < V represents near-critical homogenization to the vapor phase. Samples listed as 2Φ contained coexisting brine and vapor-rich inclusions (indicating formation in the immiscible L + V field).

[b] Pure H_2O critical point according to the IAPWS-95 equation of state (Wagner and Pruß, 2002).

[c] Experiments conducted in Au capsules.

[d] Dissolution temperature of ferrous chloride hydrate.

Pressure–temperature points along the critical isochores for 10, 15, 20, 25 and 30 wt% $FeCl_2$ compositions were identified in the present study. Fig. 2 shows an example of a typical FI from this study that homogenizes by critical behavior (fading of the meniscus between liquid and vapor) at the critical point of the fluid. During heating from room temperature to ~500 °C, there is little change in the volumetric proportion of vapor in the FI; as the FI is heated from 505 to 508 °C, the physical and optical properties of liquid and vapor converge, such that the boundary (meniscus) between the two fluids fades and vanishes at the critical point (508 °C; Fig. 2). The measured critical temperatures increase from 374 °C for pure H_2O (Wagner and Pruß, 2002) to 416, 435 and 508 °C for fluids of 10, 20 and 30 wt% $FeCl_2$, respectively (Fig. 4; Table 1).

For each bulk composition, the pressure–temperature conditions of formation of FI with the critical density are plotted on Fig. 4. Linear best-fit analysis of these *PT* points allows construction of the critical isochores. Additional constraints on the *PT* trajectories of the critical isochores were provided in some cases, as follows: Sometimes the critical isochore could be constrained by pairs of experiments from along the same isobar that were closely spaced in temperature. If such a pair of experiments resulted in FI homogenizing to the liquid in one sample, and FI homogenizing to the vapor in the other sample, then the critical isochore must pass between the *PT* conditions of these two experiments. In some experiments, all of the FI formed at different temperatures along an isobar homogenized to the liquid phase, or sometimes they all homogenized to the vapor phase. Even for such experiments useful information is provided because we know, for example, that formation conditions for which FI homogenize to the vapor phase must lie on the high-temperature/low-pressure side of the critical isochore (whereas FI homogenizing to the liquid phase imply formation on the low-temperature/high-pressure side). Thus, such experimental data provide information on the direction of temperature adjustment for subsequent experiments to determine conditions that bracket the critical isochore. After some experiments, the quartz sample contained coexisting high-salinity liquid-rich and low-salinity vapor-rich inclusions, indicating that the *PTx* conditions of those experiments were within the two-phase (immiscible L-V) field. Provided that the formation temperature was greater than the critical temperature (measured from other experiments), such conditions must lie on the high-temperature/low-pressure side of the critical isochore. All of these constraints were incorporated in the estimates of the *PT* trajectories of the critical isochores, in order to constrain conditions along the critical curve.

Extrapolation of the isochores in Fig. 4 to the measured critical homogenization temperature for each composition yields the *PTx* coordinates of a series of points along the critical curve. For pure H_2O, the critical pressure is ~220 bar (Wagner and Pruß, 2002). Based on our results, the H_2O–$FeCl_2$ critical curve extends along a sub-linear *PT* trajectory with an average dP/dT slope of ~2 bar/°C, to 475 bar at 500 °C (Figs. 4 and 5). In comparison, the critical curves of H_2O-NaCl and H_2O-KCl fluids have average dP/dT slopes of ~3 bar/°C over the same temperature range, while the critical curves of H_2O–$CaCl_2$ and H_2O–$MgCl_2$ have even steeper dP/dT slopes (Liebscher, 2007;

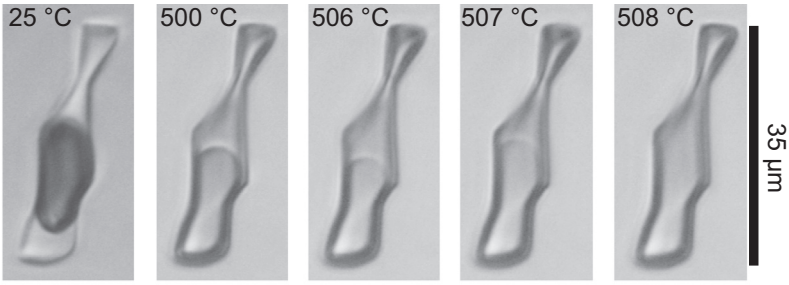

Fig. 2. Example heating sequence of an FI containing 30 wt% $FeCl_2$ that homogenizes by critical phenomena. The vapor bubble size remains essentially constant during heating from room temperature to ~500 °C; during heating from 505 to 508 °C, the meniscus dividing liquid and vapor gradually fades and vanishes.

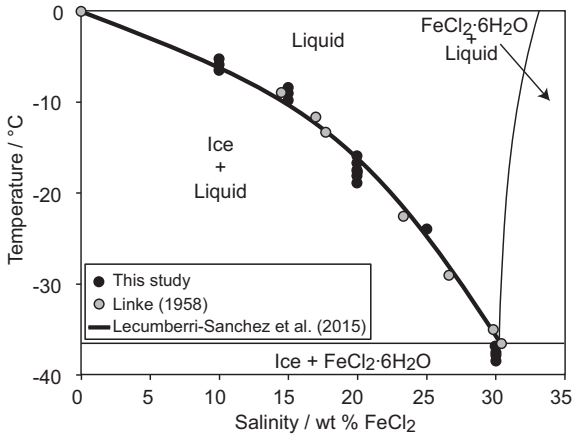

Fig. 3. Low-temperature microthermometric measurements from the present study (black circles), plotted on the vapor-saturated ice liquidus of H_2O–$FeCl_2$ according to Lecumberri-Sanchez et al. (2015). Also shown are experimental data compiled by Linke (1958) (gray circles).

Fig. 5). Thus, for any given temperature or salinity (expressed in mol% units, to exclude effects related to the different molar masses), the pressure on the critical curve increases in the order $P_{c,FeCl2} < P_{c,NaCl} < P_{c,KCl} < P_{c,MgCl2} < P_{c,CaCl2}$. To our knowledge, the critical curve for H_2O-$FeCl_2$ fluids occurs at lower pressure than any other geologically relevant H_2O-chloride salt binary system that has yet been characterized.

4. DISCUSSION

As described above, oxygen fugacity in our experiments was buffered at NNO by the pressure vessel material, and as such iron in solution was predominately in the ferrous (Fe^{2+}) state (e.g., Simon et al., 2004). It should be noted that ferric (Fe^{3+}) chloride solutions may exhibit different critical *PTx* properties, as a result of differences in the thermodynamic properties of ferric versus ferrous iron in solution (e.g., Shock et al., 1997). Thus, the critical *PTx* properties of iron-bearing fluids are expected to vary with f_{O2} as the oxidation state of iron in solution changes in response to changing f_{O2}. The *PTx* conditions along the H_2O–$FeCl_2$ critical curve described herein are expected to represent iron choride-bearing solutions throughout the range of f_{O2} in which iron occurs predominately in the ferrous state. Ferrous iron is the predominant species over approximately five orders of magnitude of f_{O2}, from one unit below the fayalite-magnetite-quartz (FMQ-1) buffer to the hematite-magnetite f_{O2} buffer (Simon et al., 2013); however, the critical *PTx* properties of iron-chloride solutions described herein are not considered to be representative of f_{O2} conditions outside this range.

4.1. H_2O–$FeCl_2$ critical curve systematics

The results of the present study suggest that the critical curve in the H_2O–$FeCl_2$ system is a continuous feature (i.e., not intersected by the three-phase L–V–S curve), at least up

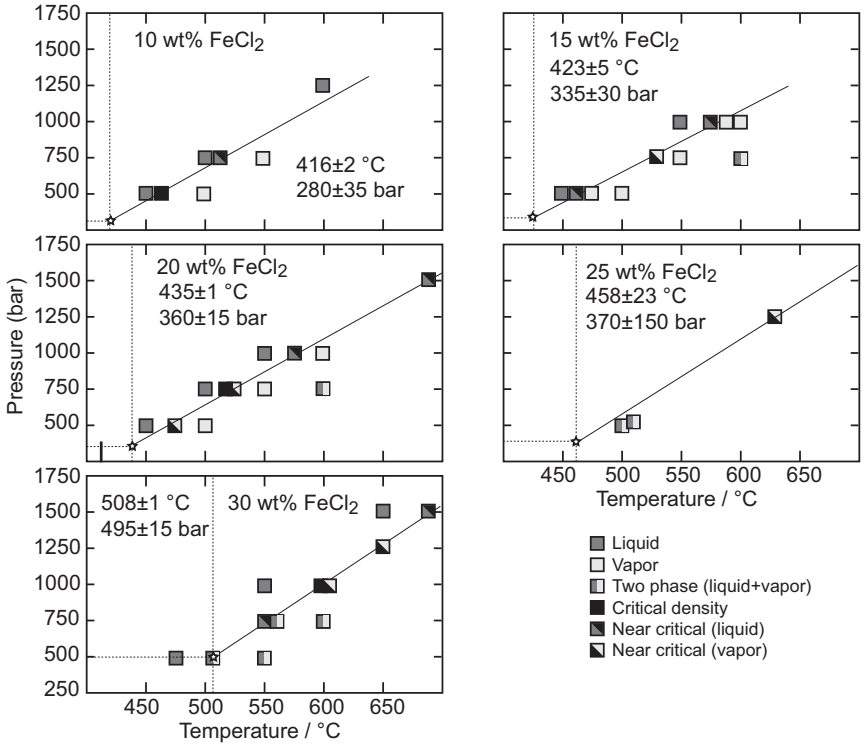

Fig. 4. Critical isochores of H_2O–$FeCl_2$ fluids containing 10, 15, 20, 25 and 30 wt% $FeCl_2$. The different square symbol styles refer to different modes of homogenization, which bracket and constrain the critical isochores. The star symbols represent the intersection of the linear best-fit through the data with the measured critical temperature. See text for additional details.

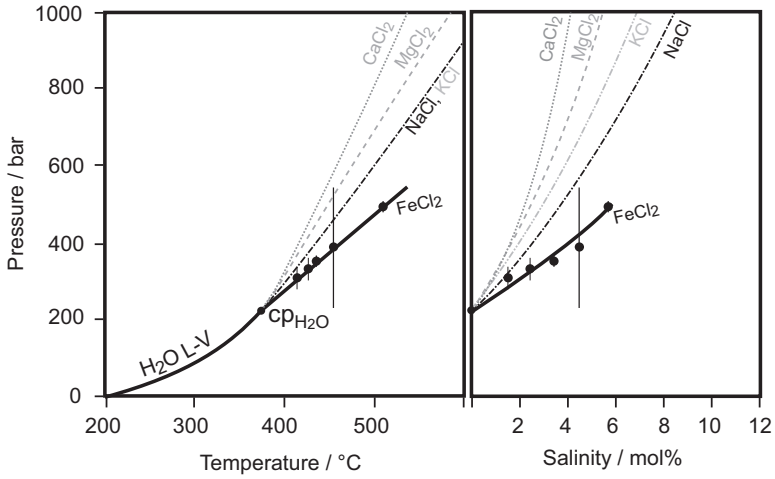

Fig. 5. Pressure-temperature and pressure-salinity projections of the critical curve of H_2O–$FeCl_2$ from the present study (symbols and thick black curve). For comparison, the critical curves of H_2O–NaCl, H_2O–KCl, H_2O–$MgCl_2$ and H_2O–$CaCl_2$ are shown, as compiled by Liebscher (2007). Note that in the PT projection, the critical curves of H_2O–NaCl and H_2O–KCl overlap almost perfectly on this scale.

to 500 °C and 30 wt% $FeCl_2$, analogous to the system H_2O–NaCl. This result was expected, because existing data indicate that $FeCl_2$ is a highly soluble salt, and the solubility of $FeCl_2$ in H_2O increases with increasing temperature (e.g., Linke, 1958). As summarized by Veksler (2004), binary H_2O–"salt" systems with these features generally exhibit an unbroken (continuous) critical curve.

As described by Levelt Sengers (1991), the initial PT trajectory of the critical curve of a binary solution (as the critical curve departs from the critical point of H_2O) is determined by the atomic-scale interactions between solute and solvent. Aqueous solutions of non-interacting solutes (such as H_2) exhibit critical curves with a nearly vertical dP/dT trend. Aqueous solutions of weakly interacting volatile solutes (such as CO_2) have critical curves with initially negative dP/dT slopes (Levelt Sengers, 1991). Aqueous solutions of highly interacting electrolyte solutes, such as alkali chlorides have critical curves that extend to the low-pressure/high-temperature side of the H_2O critical isochore (Levelt Sengers, 1991). Such electrolyte solutes are characterized by large negative partial molar volumes (e.g., Bodnar, 1985) and partial molar heat capacities at infinite dilution near the critical point of the solvent (Levelt Sengers, 1991).

Based on the considerations of solute-solvent interactions described above, the low pressure along the H_2O–$FeCl_2$ binary critical curve was at first somewhat unexpected. We had hypothesized that the critical curve PT trajectory for H_2O–$FeCl_2$ might be similar to that of binaries containing other divalent-cation chlorides such as $MgCl_2$ or $CaCl_2$. The steep dP/dT trajectories of the H_2O–$MgCl_2$ and H_2O–$CaCl_2$ critical curves imply that the solute-solvent interactions in these systems at near-critical conditions are relatively weak, compared to alkali chlorides such as NaCl and KCl (Fig. 5). Marshall and Jones (1974) and Marshall (1990) related these differences to the dissociation constants of the various salts, noting that neutral ion pairs are expected to interact only weakly with the solvent. The dissociation constant of $NaCl^0$(aq) is approximately one order of magnitude greater than that of $CaCl_2^0$(aq) at near-critical temperatures (Frantz and Marshall, 1982; Marshall, 1990). Thus, aqueous $CaCl_2$ associates more strongly than NaCl at near critical conditions. As a result, H_2O molecules are only weakly attracted to $CaCl_2^0$(aq) in solution, consistent with the greater dP/dT slope of the H_2O–$CaCl_2$ critical curve. In addition, it is noteworthy that neutral ion pairs of monovalent cation chlorides (e.g., NaCl and KCl) possess relatively strong dipole moments, whereas divalent cation chlorides such as $CaCl_2$ possess no dipole but are characterized by strong quadrupole moments (Jiang and Pitzer, 1996). The differences in ion pair polarities between monovalent versus divalent cation chlorides (even in the case of strongly ionically bonded pairs) may significantly affect the solute-solvent interactions of such species.

An additional complexity affecting interpretation of ferrous chloride–H_2O interactions arises because, unlike calcium or magnesium, iron (and other transition metals) forms charged chloride complexes at temperatures from about 200 to 450 °C, pressures of ~500 bar, and elevated chloride concentrations (e.g., $FeCl_4^{2-}$; Testemale et al., 2009). Similar chloride complexing is observed over this temperature range in solutions of manganese (Tian et al., 2014), cobalt (Liu et al., 2011), nickel (Tian et al., 2012), cadmium (Bazarkina et al., 2010) and zinc chlorides (Mayanovic et al., 1997; Liu et al., 2007). In contrast, calcium chloride solutions show $CaCl_2^0$ as the dominant species at such conditions ($\pm CaCl^+$; Frantz and Marshall, 1982; Fulton et al., 2006; Williams-Jones and Seward, 1989), and no analogous charged species of calcium chloride (e.g. $CaCl_3^-$ or $CaCl_4^{2-}$) have been detected, even at high chloride concentrations (Fulton et al., 2006). Fulton et al. (2006) suggested that the higher chlorination of transition metals compared to alkaline earths at high temperatures might reflect partially covalent bonding as a result of mixing the transition metal d orbital with the chloride p orbitals. Dissociation constants reported by Testemale et al. (2009) suggest that $FeCl_4^{2-}$ complexes may be present at

near-critical PT conditions. However, it should be noted that $FeCl_4^{2-}$ (and other highly chlorinated) complexes are favored at iron-to-chloride mole ratios in excess of 1:2 (corresponding to stoichiometric $FeCl_2$; Testemale et al., 2009), which are not present in the FI in the present study. Moreover, mass and charge balance constraints suggest that $FeCl_4^{2-}$ cannot be the predominant species in stoichiometric $FeCl_2$ solutions (which are likely dominated by neutral $FeCl_2^0$ complexes). Nevertheless, the existence of highly chlorinated complexes for transition metals, and lack thereof for alkalis and alkaline earths, suggests fundamental differences in the ligation of these metals, which may affect the respective solute-solvent interactions and critical curve trajectories.

In addition to highly chlorinated species, transition metals form a variety of solvent-stabilized, octahedrally-coordinated neutral chloride complexes (e.g., $FeCl_2(H_2O)_4^0$; Susak and Crerar, 1985). The formation and stability of such complexes also imply strong solute-solvent attraction, which in turn may contribute to the relatively low dP/dT slope of the H_2O–$FeCl_2$ critical curve. If so, then we might expect that critical curves of other aqueous transition metal chlorides (which also exhibit solvent-stabilized chloride complexes; e.g., Susak and Crerar, 1985; Bazarkina et al., 2010) may similarly have relatively low dP/dT slopes; further work is required to investigate this issue.

It should be noted that with increasing temperature above ~450 °C, $FeCl_2^0$ associates similarly to $CaCl_2^0$, and $FeCl_2^0$ is likely the predominant species throughout a wide range of magmatic-hydrothermal conditions (e.g., Heinrich and Seward, 1990; Ding and Seyfried, 1992; Fein et al., 1992; Simon et al., 2004), including the PT range of our experiments (i.e., the conditions of FI synthesis: 450–700 °C, 500–1500 bar; e.g., Chou and Eugster, 1977; Simon et al., 2004). Indeed, Chou and Eugster (1977) showed that $FeCl_2^0$ is the predominant iron species in solution at 500–650 °C and 2 kbar, while Simon et al. (2004) showed that $FeCl_2^0$ is the main aqueous iron species at 800 °C and 1–1.5 kbar. However, the key parameter affecting the PTx trajectory of the H_2O–$FeCl_2$ critical curve is the solute-solvent interaction near the critical point of H_2O (e.g., Levelt Sengers, 1991). In turn, solute-solvent interactions at such conditions are related to the near-critical speciation, which is as yet uncertain. This issue could be investigated further by applying microbeam XAFS analysis of the FI at elevated temperatures (as described by Mayanovic et al., 1997, and Anderson et al., 1998), at conditions near the critical homogenization temperature of the FI.

4.2. Applications to magmatic-hydrothermal systems

The results of this study provide quantitative constraints on the PTx extent of liquid–vapor immiscibility in iron-bearing hydrothermal fluids. As such, these results can be used to predict and interpret the PT conditions over which immiscibility might occur in magmatic-hydrothermal systems in which iron is a major fluid component. The low dP/dT slope of the H_2O-$FeCl_2$ critical curve suggests that, for iron-bearing fluids, immiscibility will occur only at relatively low pressures, or relatively shallow depths, compared to fluids rich in alkali or alkaline-earth chlorides.

Iron-rich magmatic-hydrothermal fluids have been reported in granite-related W-Sn deposits (e.g., Audétat et al., 1998, 2000; Kamenetsky et al., 2002; Seo and Heinrich, 2013). Fluid inclusions from such systems sometimes show petrographic evidence of immiscibility (coexisting vapor-rich and halite-bearing inclusions). In such cases, the pressures of formation of the host minerals cannot exceed the pressure on the critical curve for the relevant bulk composition. For example, the fluids associated with W-Sn mineralization at the Mole Granite, Australia, are iron rich and showed evidence of immiscibility (Audétat et al., 1998, 2000). The molar proportions of Na, K and Fe in the fluid were highly variable, ranging in some cases up to Fe concentrations approximately equal to those of Na and K (mole ratios Na:K:Fe approximately 1:1:1; e.g., Audétat et al., 2000; Seo and Heinrich, 2013). Thus, the maximum pressure of immiscibility is constrained by the critical curve of H_2O+(Na,K,Fe)-chloride, with the respective cation proportions. Azbej (2006) showed that the critical curves for ternary solutions of 1:1 mixtures of various chloride salts have dP/dT slopes approximated by the average of the relevant binary end-members. Therefore, if we assume that the Mole Granite fluids are approximated as H_2O–NaCl–KCl–$FeCl_2$ fluids with the molar ratio Na:K:Fe of approximately 1:1:1, then the critical curve would have a dP/dT slope of ~2.7 bar/°C. This estimate of the critical curve dP/dT slope provides an upper limit for pressure estimates in this system. For example, at 600 °C this would imply $P < 820$ bar, because above this pressure the fluid could not undergo immiscibility. At these temperatures, Audétat et al. (2000) inferred formation pressures of ~950 bar (based on PTx properties of H_2O–NaCl); thus, the results of the present study allow refinement of the pressure estimates, suggesting somewhat lower formation pressures for systems containing significant concentrations of iron.

One of the consequences of fluid phase immiscibility in hydrothermal systems is the partitioning of metals between liquid and vapor. Simon et al. (2004) previously investigated Fe partitioning between liquid and vapor for a fluid of bulk composition dominated by H_2O–NaCl, and found that at all investigated conditions, Fe was partitioned preferentially into the liquid phase (consistent with complexing of Fe by chloride; Simon et al., 2004). Although in the present study we did not measure $FeCl_2$ concentrations in coexisting liquid and vapor, some estimates may be provided based on the critical curve trajectory. Liebscher (2007) noted that liquid–vapor isotherms of H_2O–chloride salt systems, when plotted in T-x space with mole fraction as the compositional variable, have approximately equal miscibility gaps, in terms of the opening width between the liquid and vapor branches (Fig. 6). Thus, differences in chloride-salt partitioning between liquid and vapor at a given P and T can be described, to some extent, in terms of differences in the pressure and composition of the critical point on the given isotherm (Fig. 6). For example, Fig. 6 suggests that at 500 °C and 550 bar, NaCl and KCl are less strongly partitioned between liquid and vapor than $MgCl_2$ or $CaCl_2$

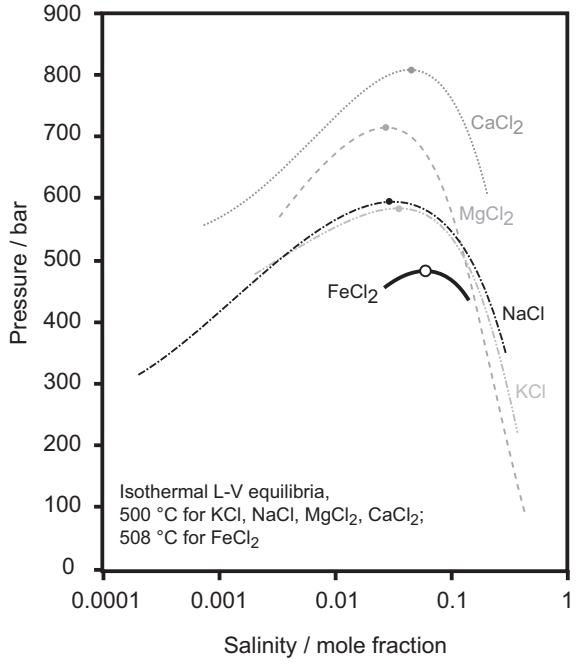

Fig. 6. Liquid–vapor isotherms of H_2O–NaCl, H_2O–KCl, H_2O–$MgCl_2$ and H_2O–$CaCl_2$ at 500 °C, compiled by Liebscher (2007). The critical point for H_2O–$FeCl_2$ at 508 °C from this study is also shown. The curvature of the liquid–vapor isotherm for H_2O–$FeCl_2$ at 508 °C is approximated, based on the isotherms of the other systems.

(i.e., the miscibility gap is narrower and the liquid and vapor branches for NaCl or KCl are closer to one another, compared to those of $MgCl_2$ or $CaCl_2$, at these conditions). If the isotherms for $FeCl_2$–H_2O indeed have a similar miscibility gap to those of the other chloride salt-water binaries, then the low pressure along the H_2O–$FeCl_2$ critical curve would suggest that $FeCl_2$ is less fractionated between liquid and vapor than NaCl would be, at a given temperature and pressure (Fig. 6). This result is consistent with the experimental results of Simon et al. (2004), which consistently showed greater fractionation of Na and K between liquid and vapor, compared to Fe. However, Audétat et al. (2000) analyzed unambiguously coexisting brine and vapor inclusions from the Mole Granite, and found that Fe is partitioned more strongly into the liquid, compared to Na. This may imply that quartz precipitation at the Mole Granite occurred at pressures significantly below the critical curve; alternatively, this may point to additional factors affecting Fe partitioning, including the role of additional ligands, especially sulfur, which is found in high concentrations in the vapor-rich inclusions from the Mole Granite (Audétat et al., 2000).

5. CONCLUSIONS

We have characterized *PTx* conditions along the critical curve of the system H_2O–$FeCl_2$, up to 30 wt% $FeCl_2$. The critical curve in the system H_2O-$FeCl_2$ occurs at lower pressure compared to those of NaCl-, KCl-, $MgCl_2$- or $CaCl_2$–H_2O fluids at any given temperature and salinity. The low-pressure trajectory of the H_2O–$FeCl_2$ critical curve suggests strong intermolecular interaction between H_2O and ferrous-chloride species in solution near the critical point of H_2O. The result allows quantitative analysis of conditions of fluid phase immiscibility in iron-rich magmatic-hydrothermal fluids, including refined interpretations of fluid inclusion data. Combining these results with known phase equilibria of H_2O-"salt"-"gas" systems provides a step towards rigorous evaluation of physical and chemical properties of complex, multicomponent fluids.

ACKNOWLEDGMENTS

This study would have been impossible without the heroic efforts of Charles Farley, who assisted in all aspects of the hydrothermal experiments, and whose help is greatly appreciated. We thank Brian Tattitch for his suggestions concerning practical aspects of iron-bearing FI synthesis. We also thank Zoltán Zajacz, Mark Frank and Adam Simon for their constructive reviews. This material is based on work supported in part by the National Science Foundation under Grant No. EAR-1019770 to R.J.B.

REFERENCES

Anderson A. J., Mayanovic R. A. and Bajt S. (1998) A microbeam XAFS study of aqueous chlorozinc complexing to 430 °C in fluid inclusions from the Knaümuhle granitic pegmatite, Saxonian granulite massif, Germany. *Can. Mineral.* **36**, 511–524.

Audétat A., Günther D. and Heinrich C. A. (1998) Formation of a magmatic-hydrothermal ore deposit: Insights with LA-ICP-MS analysis of fluid inclusions. *Science* **279**.

Audétat A., Günther D. and Heinrich C. A. (2000) Causes for large-scale metal zonation around mineralized plutons: fluid inclusion LA-ICP-MS evidence from the Mole Granite, Australia. *Econ. Geol.* **95**, 1563–1581.

Azbej T. (2006) The role of fluids in geological processes. PhD dissertation. Virginia Tech, Blacksburg, VA, p. 121.

Bazarkina E. F., Pokrovski G. S., Zotov A. V. and Hazemann J. L. (2010) Structure and stability of cadmium chloride complexes in hydrothermal fluids. *Chem. Geol.* **276**, 1–17.

Bischoff J. L. and Pitzer K. S. (1989) Liquid–vapor relations for the system NaCl–H_2O: summary of the P–T–x surface from 300–500°C. *Am. J. Sci.* **289**, 217–248.

Bodnar R. J. (1985) Pressure-Volume–Temperature-Composition (PVTX) properties of the system H_2O–NaCl at elevated temperatures and pressures. PhD dissertation, The Pennsylvania State University, University Park, PA, p. 183.

Bodnar R. J., Burnham C. W. and Sterner S. M. (1985) Synthetic fluid inclusions in natural quartz. III. determination of phase equilibrium properties in the system H_2O–NaCl to 1000 °C and 1500 bars. *Geochim. Cosmochim. Acta* **49**, 1861–1873.

Bodnar R. J., Lecumberri-Sanchez P., Moncada D. and Steele-MacInnis M. (2014) Fluid inclusions in hydrothermal ore deposits. In *Treatise on Geochemistry*, 13 (eds. H. D. Holland and K. K. Turekian). Elsevier, Oxford, pp. 119–142 (second ed.).

Bodnar R. J. and Sterner S. M. (1987) Synthetic fluid inclusions. In *Hydrothermal Experimental Techniques* (eds. G. C. Ulmer and H. L. Barnes). Wiley-Interscience, New York, pp. 423–457.

Bowen N. L. and Schairer J. F. (1932) The system FeO–SiO_2. *Am. J. Sci.* **24**, 177–213.

Chou I. M. and Eugster H. P. (1977) Solubility of magnetite in supercritical chloride solutions. *Am. J. Sci.* **277**, 1296–1314.

Ding K. and Seyfried W. E. (1992) Determination of Fe–Cl complexing in the low pressure supercritical region (NaCl fluid): iron solubility constraints on pH of subsea floor hydrothermal fluids. *Geochim. Cosmochim. Acta* **56**, 3681–3692.

Driesner T. and Heinrich C. A. (2007) The system H_2O–NaCl. Part I: correlation formulae for phase relations in temperature–pressure-composition space from 0 to 1000 °C, 0 to 5000 bar, and 0 to 1 X_{NaCl}. *Geochim. Cosmochim. Acta* **71**, 4880–4901.

Drummond S. E. and Ohmoto H. (1980) Chemical evolution and mineral deposition in boiling hydrothermal systems. *Econ. Geol.* **80**, 126–147.

Dubois M., Weisbrod A. and Shtuka A. (1994) Experimental determination of the two-phase (liquid and vapour) region in water-alkali chloride binary systems at 500 and 600 °C using synthetic fluid inclusions. *Chem. Geol.* **115**, 227–238.

Esposito R., Klebesz R., Bartoli O., Klyukin Y. I., Moncada D., Doherty A. and Bodnar R. J. (2012) Application of the Linkam TS1400XY heating stage to melt inclusion studies. *Central Eur. J. Geosci.* **4**, 208–218.

Eugster H. P. and Skippen B. (1967) Igneous and metamorphic reactions involving gas equilibria. In *Researches in Geochemistry, II* (ed. P. H. Ableson). John Wiley & Sons, New York, pp. 492–520.

Fein J. B., Hemley J. J., D'Angelo W. M., Komninou A. and Sverjensky, D.A., 1992. Experimental study of iron-chloride complexing in hydrothermal fluids. *Geochim. Cosmochim. Acta* **56**.

Frank M., Candela P. A., Piccoli P. M. and Glascock M. D. (2001) Gold solubility, speciation and partitioning as a function of HCl in the brine-silicate melt-metallic gold system at 800 °C and 100 MPa. *Geochim. Cosmochim. Acta* **66**, 3719–3732.

Frantz J. D. and Marshall W. L. (1982) Electrical conductances and ionization constants of calcium chloride and magnesium chloride in aqueous solutions at temperatures to 600 °C and pressures to 4000 bars. *Am. J. Sci.* **282**, 1666–1693.

Fulton J. L., Chen Y., Heald S. M. and Balasubramanian M. (2006) Hydration and contact ion pairing of Ca^{2+} with Cl in supercritical aqueous solution. *J. Chem. Phys.* **125**, 094501–094510.

Grant J. N., Halls C., Avila W. and Avila G. (1977) Igneous geology and the evolution of hydrothermal systems in some sub-volcanic tin deposits of Bolivia. *Geol. Soc. London Special Publ.* **7**, 117–126.

Günther D., Audétat A., Frischknecht A. and Heinrich C. A. (1998) Quantitative analysis of major, minor, and trace elements in fluid inclusions using laser ablation-inductively coupled plasma mass spectrometry. *J. Anal. At. Spectrom.* **13**, 263–270.

Hanley J. J., Mungall J. E., Pettke T., Spooner E. T. C. and Bray C. J. (2005) Ore metal redistribution by hydrocarbon-brine and hydrocarbon-halide melt phases, North Range footwall of the Sudbury Igneous Complex, Ontario, Canada. *Miner. Deposita* **40**, 237–256.

Hedenquist J. W., Arribas A. and Reynolds T. J. (1998) Evolution of an intrusion-centered hydrothermal system: far Southeast-Lepanto porphyry and epithermal Cu–Au deposits, Phillipines. *Econ. Geol.* **93**, 373–404.

Hedenquist J. W. and Lowenstern J. B. (1994) The role of magmas in the formation of hydrothermal ore deposits. *Nature* **370**, 519–527.

Heinrich C. A. and Seward T. M. (1990) A spectrophotometric study of aqueous iron (II) chloride complexing from 25 to 200 °C. *Geochim. Cosmochim. Acta* **54**, 2207–2221.

Jiang S. and Pitzer K. S. (1996) Phase equilibria and volumetric properties of aqueous $CaCl_2$, by an equation of state. *AIChE J.* **42**, 585–594.

Kamenetsky V. S., van Achterbergh E., Ryan C., Naumov V. B., Mernagh T. P. and Davidson P. (2002) Extreme chemical heterogeneity of granite-derived hydrothermal fluids: an example from inclusions in a single crystal of miarolitic quartz. *Geology* **30**.

Knight C. L. and Bodnar R. J. (1989) Synthetic fluid inclusions. IX. Critical PVTX properties of NaCl–H_2O solutions. *Geochim. Cosmochim. Acta* **53**, 3–8.

Lecumberri-Sanchez P., Steele-MacInnis M. and Bodnar R. J. (2015) Synthetic fluid inclusions XIX. Experimental determination of the vapor-saturated liquidus of the system H_2O–NaCl–$FeCl_2$. *Geochim. Cosmochim. Acta* **148**, 34–49.

Levelt Sengers J. M. H. (1991) Solubility near the solvent's critical point. *J. Supercrit. Fluids* **4**, 215–222.

Liebscher A. (2007) Experimental studies in model fluid systems. *Rev. Mineral. Geochem.* **65**, 15–47.

Linke W. (1958) *Solubilities, Inorganic and Metal Organic Compounds*. D. Van Nostrand Company, Princeton, New Jersey.

Liu W. H., Borg S. J., Testemale D., Etschmann B., Hazemann J. L. and Brugger J. (2011) Speciation and thermodynamic properties for cobalt chloride complexes in hydrothermal fluids at 35–440 °C and 600 bar: an in-situ XAS study. *Geochim. Cosmochim. Acta* **75**, 1227–1248.

Liu W. H., Etschmann B., Foran G., Shelley M. and Brugger J. (2007) Deriving formation constants for aqueous metal complexes from XANES spectra: Zn^{2+} and Fe^{2+} chloride complexes in hypersaline solutions. *Am. Mineral.* **92**, 761–770.

Marshall W. L. (1990) Critical curves of aqueous electrolytes related to ionization behaviour: new temperatures for sodium chloride solutions. *J. Chem. Soc., Faraday Trans.* **86**, 1807–1814.

Marshall W. L. and Jones E. V. (1974) Liquid-vapor critical temperatures of aqueous electrolyte solutions. *J. Inorg. Nucl. Chem.* **36**, 2313–2318.

Mayanovic R. A., Anderson A. J. and Bajt S. (1997) Microbeam XAFS studies on fluid inclusions at high temperatures. *J. Phys. IV* **7**, 1029–1030.

Moncada D., Mutchler S., Nieto A., Reynolds T. J., Rimstidt J. D. and Bodnar R. J. (2012) Mineral textures and fluid inclusion petrography of the epithermal Ag–Au deposits at Guanajuato, Mexico: application to exploration. *J. Geochem. Explor.* **114**, 20–35.

Oakes C. S., Bodnar R. J., Simonson J. M. and Pitzer K. S. (1994) Critical and supercritical properties for 0.3–3.0 mol kg^{-1} $CaCl_2$(aq). *Geochim. Cosmochim. Acta* **58**, 2421–2431.

Pester N. J., Rough M., Ding K. and Seyfried W. E. (2011) A new Fe/Mn geothermometer for hydrothermal systems: implications for high-salinity fluids at 13°N on the East Pacific Rise. *Geochim. Cosmochim. Acta* **75**, 7881–7892.

Popp R. K., Nagy K. L. and Hajash A. (1984) Semiquantitative control of hydrogen fugacity in rapid-quench hydrothermal vessels. *Am. Mineral.* **69**, 557–562.

Roedder E. (1984) Fluid inclusions. *Rev. Mineral.* **12**, 644.

Schimmel F. (1928) Löslichkeiten und Umwandlungspunkte der Eisenchlorürhydrate in wäßriger Lösung. *Z. Anorg. Allg. Chem.* **173**, 285–288.

Seo J. H. and Heinrich C. A. (2013) Selective copper diffusion into quartz-hosted vapor inclusions: evidence from other host minerals, driving forces, and consequences for Cu–Au ore formation. *Geochim. Cosmochim. Acta* **113**, 60–69.

Shmulovich K. I., Tkachenko S. I. and Plyasunova N. V. (1995) Phase equilibria in fluid systems at high pressures and temperatures. In *Fluids in the Crust: Equilibrium and Transport Properties* (eds. K. I. Shmulovich, B. W. D. Yardley and G. G. Gonchar). Chapman & Hall, London, pp. 193–214.

Shock E. L., Sassani D. C., Willis M. and Sverjensky D. A. (1997) Inorganic species in geologic fluids: correlations among

standard molal thermodynamic properties of aqueous ions and hydroxide complexes. *Geochim. Cosmochim. Acta* **61**, 907–950.

Simon A. C., Pettke T., Candela P. A., Piccoli P. M. and Heinrich C. A. (2004) Magnetite solubility and iron transport in magmatic-hydrothermal environments. *Geochim. Cosmochim. Acta* **23**, 4905–4914.

Simon A., Bilenker L. and Bell A. (2013) The importance of iron mobility in magmatic-hydrothermal systems. *Mineral. Magazine* **77**, 2215.

Souririjan S. and Kennedy G. C. (1962) The system H_2O–NaCl at elevated temperatures and pressures. *Am. J. Sci.* **260**, 115–141.

Sterner S. M. and Bodnar R. J. (1984) Synthetic fluid inclusions in natural quartz. I. Compositional types synthesized and applications to experimental geochemistry. *Geochim. Cosmochim. Acta* **48**, 2659–2668.

Susak N. J. and Crerar D. A. (1985) Spectra and coordination changes of transition metals in hydrothermal solutions: implications for ore genesis. *Geochim. Cosmochim. Acta* **49**, 555–564.

Testemale D., Brugger J., Liu W. H., Etschmann B. and Hazemann J. L. (2009) In-situ X-ray absorption study of iron(II) speciation in brines up to supercritical conditions. *Chem. Geol.* **264**, 295–310.

Tian Y., Etschmann B., Liu W. H., Borg S., Mei Y., Testamale D., O'Neill B., Rae N., Sherman D. M., Ngothai Y., Johanessen B., Glover B. and Brugger J. (2012) Speciation of nickel (II) chloride complexes in hydrothermal fluids: in situ XAS study. *Chem. Geol.* **334**, 345–363.

Tian Y., Etschmann B., Mei Y., Grundler P. V., Testemale D., Hazemann J. L., Elliott P., Ngothai Y. and Brugger J. (2014) Speciation and thermodynamic properties of manganese(II) chloride complexes in hydrothermal fluids: in situ XAS study. *Geochim. Cosmochim. Acta* **129**, 77–95.

Valyashko V. M. (2014) Phase equilibria in binary and ternary hydrothermal systems. In *Hydrothermal Properties of Materials* (ed. V. M. Valyashko). John Wiley & Sons, New York, pp. 2–133.

Veksler I. V. (2004) Liquid immiscibility and its role at the magmatic-hydrothermal transition: a summary of experimental studies. *Chem. Geol.* **210**, 7–31.

Wagner W. and Pruß A. (2002) The IAPWS formulation 1995 for the thermodynamic properties of ordinary water substance for general and scientific use. *J. Phys. Chem. Ref. Data* **31**, 387–535.

Werre R. W., Bodnar R. J., Bethke P. M. and Barton P. B. (1979) A novel gas-flow fluid inclusion heating/freezing stage. *Geol. Soc. Am. Abstr. Prog.* **11**, 539.

Williams-Jones A. E. and Seward T. M. (1989) The stability of calcium chloride ion pairs in aqueous solutions at temperatures between 100 and 360 °C. *Geochim. Cosmochim. Acta* **53**, 313–318.

Yardley B. W. D. (2005) Metal concentrations in crustal fluids and their relationship to ore formation. *Econ. Geol.* **100**, 613–632.

Yardley B. W. D. and Bodnar R. J. (2014) Fluids in the continental crust. *Geochem. Perspect.* **3**, p. 127.

Zajacz Z., Seo J. H., Candela P. A., Piccoli P. M. and Tossell J. A. (2011) The solubility of copper in high-temperature magmatic vapors: a quest for the significance of various chloride and sulfide complexes. *Geochim. Cosmochim. Acta* **75**, 2811–2827.

Associate editor: Edward M. Ripley